Cerebral Cortex, January 2021;31: 439–447

doi: 10.1093/cercor/bhaa235
Advance Access Publication Date: 8 September 2020
Original Article

ORIGINAL ARTICLE

Ultrahigh-resolution MRI Reveals Extensive Cortical Demyelination in a Nonhuman Primate Model of Multiple Sclerosis

Maxime Donadieu[1], Hannah Kelly[1], Diego Szczupak[2], Jing-Ping Lin[1], Yeajin Song[1], Cecil C.C. Yen[3], Frank Q. Ye[4], Hadar Kolb[1], Joseph R. Guy[1], Erin S. Beck[1], Steven Jacobson[5], Afonso C. Silva[2], Pascal Sati[1] and Daniel S. Reich[1]

[1]Translational Neuroradiology Section, National Institute of Neurological Disorders and Stroke, National Institutes of Health, Bethesda, MD 20892, USA, [2]Department of Neurobiology, University of Pittsburgh, Pittsburgh, PA 15261, USA, [3]Cerebral Microcirculation Section, Laboratory of Functional and Molecular Imaging, National Institute of Neurological Disorders and Stroke, National Institutes of Health, Bethesda, MD 20892, USA, [4]Neurophysiology Imaging Facility, National Institute of Mental Health, National Institutes of Health, Bethesda, MD 20892, USA and [5]Viral Immunology Section, National Institute of Neurological Disorders and Stroke, National Institutes of Health, Bethesda, MD 20892, USA

Address correspondence to Dr Daniel S. Reich, National Institute of Neurological Disorders and Stroke, 10 Center Drive, Building 10, Room 5C103, Bethesda, MD 20814, USA. Email: daniel.reich@nih.gov.

Abstract

Cortical lesions are a primary driver of disability in multiple sclerosis (MS). However, noninvasive detection of cortical lesions with in vivo magnetic resonance imaging (MRI) remains challenging. Experimental autoimmune encephalomyelitis (EAE) in the common marmoset is a relevant animal model of MS for investigating the pathophysiological mechanisms leading to brain damage. This study aimed to characterize cortical lesions in marmosets with EAE using ultrahigh-field (7 T) MRI and histological analysis. Tissue preparation was optimized to enable the acquisition of high-spatial resolution (50-µm isotropic) T_2^*-weighted images. A total of 14 animals were scanned in this study, and 70% of the diseased animals presented at least one cortical lesion on postmortem imaging. Cortical lesions identified on MRI were verified with myelin proteolipid protein immunostaining. An optimized T_2^*-weighted sequence was developed for in vivo imaging and shown to capture 65% of cortical lesions detected postmortem. Immunostaining confirmed extensive demyelination with preserved neuronal somata in several cortical areas of EAE animals. Overall, this study demonstrates the relevance and feasibility of the marmoset EAE model to study cortical lesions, among the most important yet least understood features of MS.

Key words: demyelination, EAE, marmoset, MRI, multiple sclerosis

Introduction

Multiple sclerosis (MS) is a chronic inflammatory disease of the central nervous system (CNS) affecting more than 2 million people worldwide, which remains incurable despite the growing number of treatments (Ascherio and Munger 2016). MS is characterized by inflammatory demyelinated lesions disseminated throughout the CNS (Reich et al. 2018). White matter (WM)

lesions are the most studied pathological feature of MS and can be readily assessed noninvasively using magnetic resonance imaging (MRI). However, demyelinated lesions are not limited to WM and can also frequently involve deep and cortical gray matter (GM). GM lesions in MS patients have been classified morphologically into subpial, intracortical, and leukocortical subtypes (Bø et al. 2003; Kutzelnigg and Lassmann 2005; Lucchinetti et al. 2011), and together these are thought to be a primary driver of disability and progression in MS (Calabrese et al. 2012). Unfortunately, the detection of cortical lesions routinely in patients using MRI remains challenging, which limits the ability to study their dynamics. Specifically, insufficient spatial resolution (even at 1-mm isotropic), poor tissue contrast due to low levels of inflammation and demyelination, and partial volume effects with surrounding cerebrospinal fluid, all hamper the in vivo detection of cortical lesions.

For these reasons, understanding cortical lesions would benefit from an animal model of MS in which imaging approaches can be developed and validated histopathologically. Experimental autoimmune encephalomyelitis (EAE) in rodents is the gold standard in the field of MS-like animal models (Burrows et al. 2019). Although MRI in mice and rats is straightforward, these animals tend to develop demyelinated lesions mostly in the spinal cord and only rarely in the cortex. On the other hand, EAE in the common marmoset (*Callithrix jacchus*) shares remarkable pathological and radiological similarities with MS with respect to WM pathology and is an excellent model to study lesion formation and evolution in the brain and spinal cord ('t Hart and Massacesi 2009; Maggi et al. 2014, 2017; Absinta et al. 2016; Lefeuvre et al. 2019). Although cortical demyelination has been demonstrated previously in marmosets with EAE (Pomeroy et al. 2008, 2010; Kramann et al. 2015), it has not been investigated by MRI. Based on previous human studies at ultrahigh field (7 T), T_2*-weighted images have been shown to detect different types of cortical lesions (Mainero et al. 2009; Pitt et al. 2010; Cohen-Adad et al. 2011). Indeed, T_2*-weighted images offer suitable GM/WM contrast and are sensitive to small changes in uniformity in the magnetic field related to inflammation, demyelination, and changes in iron concentration (Tang et al. 2014; Stüber et al. 2016).

Therefore, the aim of this study was to investigate whether cortical lesions can be accurately visualized by postmortem and in vivo T_2*-weighted MRI in marmoset EAE.

Material and Methods

EAE Induction

All marmosets (*C. jacchus*) used in this study were housed in the National Institutes of Health (NIH) Intramural Research Program facilities, following the standards of the American Association for Accreditation of Laboratory Animal Care and the National Institute of Neurological Disorders and Stroke (NINDS) Animal Care and Use Committee (ACUC).

Half-brains from 12 animals (mean age = 5.7 years [range 1.5–12.1]; 7 left and 5 right hemispheres; 10 females and 2 males) were prepared and scanned using postmortem MRI. In nine of these animals (Table 1, M1–M9), EAE was induced with 200 mg of human white matter (hWM) collected from a healthy donor. Briefly, hWM was emulsified in complete Freund's adjuvant in a 1:1 volumetric ratio containing 1.8-mg desiccated *Mycobacterium tuberculosis*. A total of 600 µL of hWM homogenate was split and injected into four dorsal sites around the lymph nodes as a part of previous studies performed in our laboratory (Lee et al. 2018; Lefeuvre et al. 2019). Two animals, denoted M12 and M13, were also studied with postmortem MRI as control animals.

Three animals (Table 1, mean age = 6 years old [3.1, 7.3, and 7.5], all female) were randomly selected from the colony. These animals, denoted M10, M11, and M14, were used for the in vivo studies. In order to reduce avoidable skin irritation caused by tuberculosis and mitigate hWM batch variance from donor to donor, two of them (M10 and M11) were immunized with 200 µg of recombinant human myelin oligodendrocyte glycoprotein (1–125, AS-55158-1000, AnaSpec) emulsified with incomplete Freund's adjuvant (Difco adjuvant, 263 910, BD) in a 1:1 volumetric ratio. A total of 200-µL homogenate was split and injected into four dorsal sites around the lymph nodes. M14 was a control animal. M10 was the only animal scanned using in vivo and postmortem MRI. M11 was not scanned postmortem, as the brain was used for another study.

All animals were scored before sacrifice (decided following the ACUC guidelines when either the body weight decreases more than 10%, both legs are paralyzed, or the animal experiences severe hypothermia) using a previously published EAE scale based on clinical symptoms, with scores ranging from 0 (no symptoms) to 45 (death) (Villoslada et al. 2000).

Postmortem Sample Preparation

All brains were perfused transcardially with 4% paraformaldehyde during necropsy, postfixed in 10% neutral buffered formalin, and scanned with and without gadolinium-based preparation (Guy et al. 2016). This preparation consisted of soaking the half-brains in 50-mL deionized water and 0.2-mL gadobutrol (Gadavist, Bayer) for 10 days in order to shorten the T_1 relaxation times of the tissues. This reduction in T_1 relaxation time enables the use of shorter repetition time (TR) and thus increases the signal-to-noise (SNR) ratio by allowing more acquisitions in a given total scan time (Supplementary Fig. S1). Before scanning, samples were secured to an in-house-designed 3D printed holder (Luciano et al. 2016), positioned inside a plastic tube filled with Fomblin (Solvay), and inserted into a 30-mm inner diameter quadrature coil (Millipede coil, ExtendMR LLC).

Postmortem MRI

Postmortem imaging was performed on a Bruker Biospec 7 T/30 cm (Bruker). After running a localizer (three planes, one slice per plane) in order to position the tissue at the isocenter of the magnet, a 3D T_2*-weighted gradient echo sequence was performed overnight to obtain images with high SNR (time echo [TE] = 34 ms; TR = 62 ms; flip angle [FA] = 75°; voxel size = 50-µm isotropic; field of view [FOV] = 16 × 35 × 25 mm; matrix = 320 × 700 × 500; number of acquisitions = 6; acquisition time [AT] = 2 h 10 min per acquisition, ≈13 h total).

In Vivo MRI

In vivo brain imaging was performed on two EAE animals (M10 and M11) and one naïve animal (M14) on the same scanner using an 8-channel receiver coil built in-house (Papoti et al. 2017). After running a localizer (three planes, one slice per plane), a whole-brain high-resolution T_1-weighted sequence (TE = 3.5 ms; TR = 6000 ms; inversion time = 1200 ms; in-plane resolution = 150 × 150 µm; thickness = 1 mm; FOV = 32 × 24 × 36 mm; matrix = 213 × 160 × 36; FA = 7°; number of acquisitions = 4;

Table 1 Demographic and clinical information of the 14 marmosets (M) used in this study

Animals	Sex	Age (years)	MRI (hemisphere)	Experiment duration[a] (weeks)	EAE score[b]	First lesion appearance[c] (weeks)
M1	F	12.1	PM (left)	18	41	11
M2	F	6.7	PM (right)	268	28	8
M3	F	3.2	PM (left)	5	18	2
M4	F	4.3	PM (left)	12	11	3
M5	F	4.5	PM (right)	4	10	3
M6	F	1.5	PM (left)	31	8	No WM lesion
M7	F	9.6	PM (right)	15	17	No WM lesion
M8	F	4.8	PM (left)	10	18	7
M9	M	3	PM (right)	16	41	11
M10	M	7.3	In vivo/PM (right)	7	24	5
M11	F	7.7	In vivo	7	28	5
M12	F	5.9	PM (left)	NA	0	NA
M13	F	4.9	PM (left)	NA	0	NA
M14	F	3.1	In vivo	NA	0	NA

Note: F, female; M, male; PM, postmortem.
[a]Experiment duration from EAE induction to sacrifice.
[b]EAE score at the terminal day. See Villoslada et al. 2000.
[c]Time between EAE immunization and first WM lesions on MRI.

AT = 28 min total), used as an anatomical reference, and a 3D flow-compensated T_2*-weighted gradient echo sequence, covering from the very top part of the brain to the beginning of the temporal lobes (TE = 25 ms; TR = 60 ms; FA = 14°; voxel size = 125-µm isotropic; FOV = 32 × 10 × 36 mm; matrix = 255 × 80 × 287; number of acquisitions = 6; AT = 11 min per acquisition, ≈1 h total), were performed.

Image Analysis

Images were analyzed using software adapted for MRI image processing: Medical Image Processing, Analysis and Visualization (NIH) and custom routines written in Matlab (MathWorks). For each animal, postmortem MRI images were coregistered to the first acquisition and averaged to maximize the SNR. In vivo T_2*-weighted gradient echo volumes were coregistered to the in vivo T_1-weighted volumes and averaged to maximize the SNR. Cortical GM lesions were manually segmented using ITK-SNAP software (Version 3.8.0) by two experts (E.S.B., a neurologist with 4 years of experience in image analysis, and M.D., an MRI physicist with 5 years of experience in image analysis) on the postmortem T_2*-weighted average images for each animal and on in vivo images for M10. Lesions were defined as hyperintense voxels on T_2*-weighted images and visible on at least two contiguous coronal images. Cortical lesions were classified into three different types: leukocortical lesions (involving both WM and cortex), intracortical lesions (small round lesions located entirely within cortical GM and not touching the WM or pial borders) and subpial lesions (large lesions involving the outermost layers of the cortex) (Dutta and Trapp 2007). The number of lesions was counted for each animal on postmortem images, and lesion volume was determined using Matlab (R2018a). Also, WM lesion burden was qualitatively evaluated on postmortem T_2*-weighted images by two experts with more than 5 years of experience in MS and image analysis (H.K., a neurologist, and M.D.) and classified as: 1—none; 2—low, with small focal lesions in different WM areas, but no confluent lesions; 3—moderate, with approximately 25–50% of the WM involved, including confluent lesions in some WM areas; and 4—high, with approximately 50–100% of the WM involved, including confluent lesions in many WM areas.

Histology

Postmortem MRI was used to target cortical lesions with a variety of types, sizes, and locations. Three-millimeter thick slabs were cut from each marmoset brain following a previously published procedure (Luciano et al. 2016). These slabs were paraffin-embedded before sectioning into 5-µm thick sections using a microtome (Leica RM2235, Leica Biosystems). To assess the level of demyelination and the level of neuronal injury in the cortex, co-staining using antibodies against myelin proteolipid protein (PLP, Bio-Rad MCA839G) and NeuN (Abcam ab104225) was performed as follows: Sections were deparaffinized and rehydrated before being rinsed in triphosphate-buffered saline for 10 min each and then processed for antigen retrieval (HIER, heat-induced epitope retrieval), followed by treatment in 0.3% endogenous peroxidase blocking for 10 min. The sections were blocked with a protein blocking solution for 10 min and incubated with the primary antibodies for 60 min at room temperature. The sections were then rinsed and incubated with secondary antibodies for 30 min. DiaminoBenzidine horseradish peroxidase for PLP development and Vector Blue Alkaline Phosphatase for NeuN development were used. Stained sections were digitally scanned with a Nikon microscope (Nikon Ci-L Multi-Headed Microscope with 5.9 MP Camera System).

MRI–Histopathology Evaluation

PLP/NeuN-stained sections were selected based on the lesion locations on postmortem MRI and visually matched with MRI images using anatomical landmarks. For M10, for which in vivo and postmortem images were obtained, both image types and PLP/NeuN-stained sections were visually matched in the same way. Five immunostained sections (5-µm thick) from four EAE animals (M1, M9, M10, and one EAE animal without cortical lesions, M4) and one control (M12) were reviewed by a consensus of two raters with experience in MS imaging and pathology

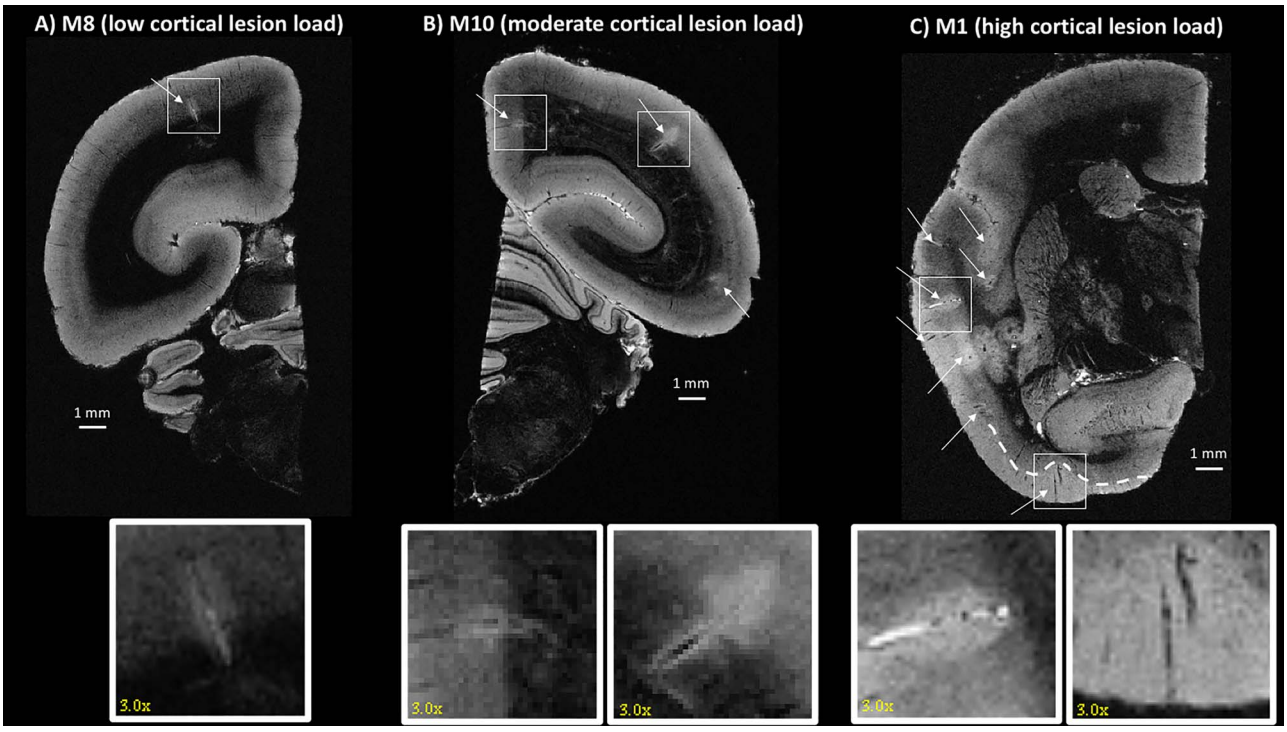

Figure 1. Postmortem 3D T_2*-weighted gradient echo MRI showing different types of cortical lesions detected in three different animals (from low to high cortical lesion load). White arrows point to identified cortical lesions. (*A*) One leukocortical lesion (box) was identified in M8 in the occipital cortex. (*B*) Two leukocortical lesions were identified in M10 in the parietal cortex and the cingulate cortex (boxes). (*C*) M1 had many cortical lesions, including intracortical and subpial (boxes). The white dashed line shows the extent of the subpial lesion. All lesions are magnified by a factor of three in the inset.

(H.K. and M.D.), disagreements were discussed, and comments were recorded. Cortical lesions were defined as well-demarcated areas of demyelination, with loss of normal PLP staining. To match the MRI classification, cortical lesions were classified into leukocortical, intracortical, and subpial subtypes (Dutta and Trapp 2007). For each section, cortical lesions were classified and counted, providing a total lesion number for each group. Juxtacortical lesions (WM lesions abutting, but not entering, the cortical mantle) were not counted.

Results

Characteristics of Animals with EAE

All immunized animals developed clinical symptoms (ranging from a slight loss of strength in the arms, legs, and tail to complete lower body paralysis and blindness) and presented an average EAE score of 22 at the time of sacrifice (range 8–41). The median time from immunization to sacrifice was 12 weeks across the nine animals (range 4–31). One animal had an exceptionally long disease duration of 268 weeks (M2). The median age at sacrifice was 4.8 years (range 3–12.1) (Table 1).

No brain abnormalities were observed on MRI in the control animals. In two animals with EAE (M6 and M7), no WM lesions were seen on postmortem MRI. Four animals (M3, M4, M5, and M9) had a low level of WM lesions on postmortem MRI, two animals (M2 and M8) had a moderate level of WM lesions, and two animals (M1 and M10) had a high level of WM lesions. For the eight animals that developed WM lesions, the median time from EAE immunization to first WM lesion appearance on in vivo MRI was 6 weeks (range 2–11 weeks).

Quantification of Cortical Lesions Using Postmortem MRI

Of the 10 animals with EAE scanned postmortem, three (M4, M5, and M6) did not have any identifiable cortical lesions on ultrahigh-resolution T_2*-weighted images. Seven animals (M1, M2, M3, M7, M8, M9, and M10) had at least one cortical lesion (Figs 1 and 2). Control animals did not have any cortical abnormalities on postmortem images. Three animals (M3, M7, and M8) had fewer than five cortical lesions, which were leukocortical or intracortical with a relatively low total volume (0.08, 0.03, and 1.3 µL, respectively); these animals had relatively low EAE scores (18, 17, and 18, respectively). Two animals (M2 and M10) had 10–20 cortical lesions, which were either leukocortical or intracortical, with a respective total volume of 0.61 and 23.3 µL and EAE scores of 28 and 24, respectively. Finally, two animals (M1 and M9) each had more than 20 cortical lesions, which were classified into three different subtypes (leukocortical, intracortical, and subpial); total cortical lesion volume was high in these animals (139 µL and 1.0 mL, respectively), as were EAE scores (41 for both animals) (Fig. 2).

In Vivo MRI Detection of Cortical Lesions

Images acquired in vivo from the control animal did not have any cortical abnormalities. The two EAE animals imaged in vivo (M10 and M11) had at least one cortical lesion each. M11 showed only one leukocortical lesion in the right hemisphere but was not scanned postmortem, as the brain was used for another study in the laboratory. A total of 12 leukocortical lesions were detected in vivo in the right hemisphere of M10 compared

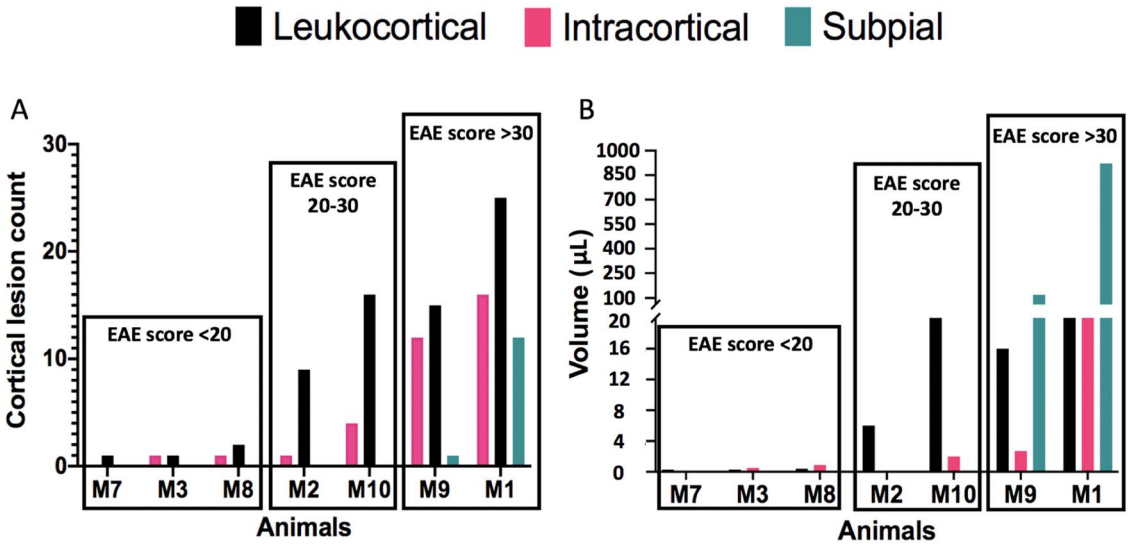

Figure 2. Bar graphs presenting the count (*A*) and the volume (*B*) of each subtype of cortical lesions detected in EAE animals (from low to high cortical lesion load, dark green: subpial; black: leukocortical; pink: intracortical). Animals are subdivided into three groups, depending on their EAE scores: <20, 20–30, and >30.

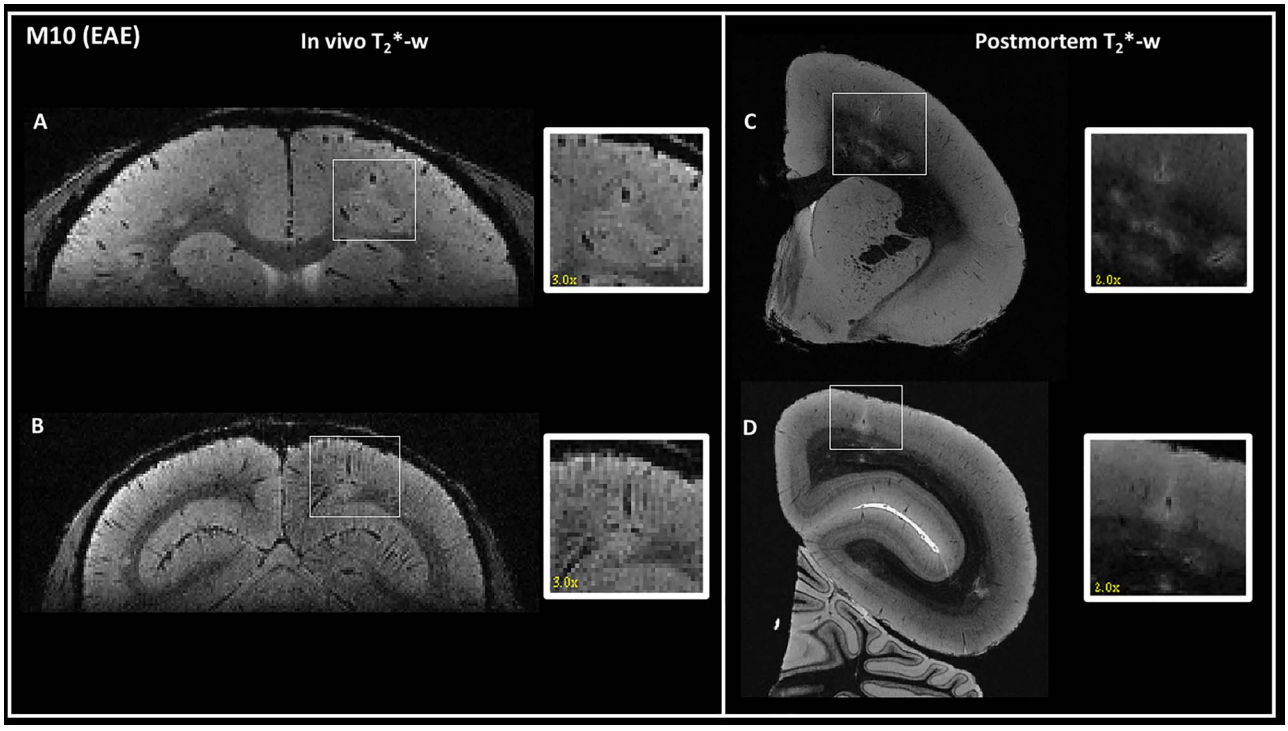

Figure 3. Detection of the same cortical lesions in one EAE animal (M10) using in vivo (left) and postmortem (right) 3D T_2*-weighted gradient-echo sequences. One intracortical (*A*) and one leukocortical (*B*) lesions were detected in vivo in two different areas: (*A*) right parietal cortex and (*B*) right occipital cortex. The same lesions were identified on postmortem MRI (*C* and *D*). In vivo lesions are magnified by a factor of three and postmortem lesions by a factor of two in the inset. Interestingly, cortical lesions appear larger in the in vivo images compared with postmortem images, likely due to water shifts.

with 17 leukocortical lesions detected on postmortem MRI (71% sensitivity). Two intracortical lesions were detected in vivo in the right hemisphere of M10 compared with four in the right hemisphere on postmortem MRI (50% sensitivity) (Fig. 3). No subpial lesions were detected on in vivo or postmortem MRI in the right hemisphere of M10. In the left hemisphere, which was not available for postmortem MRI analysis, in vivo MRI showed 16 cortical lesions, of which 13 were leukocortical, three intracortical, and zero subpial.

Validation of MRI Findings by Histopathology

A healthy animal (M12) displayed normal WM and GM signal on MRI and normal PLP/NeuN staining. All subtypes of cortical

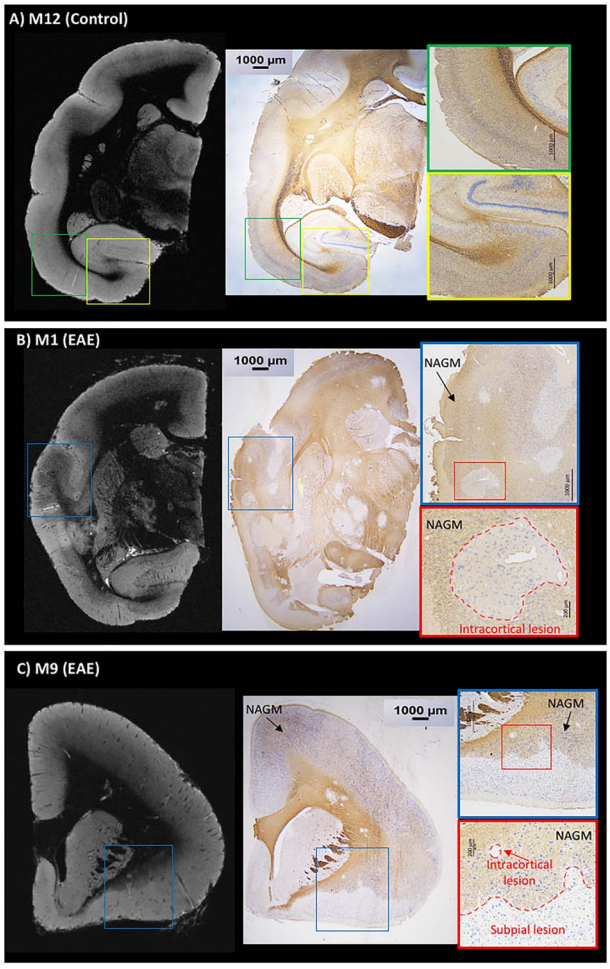

Figure 4. Postmortem T_2*-weighted gradient echo MRI and PLP/NeuN immunohistochemistry are well correlated. (*A*) Control animal (M12) with normal MRI contrast and normal PLP/NeuN staining. PLP (brown) staining is darker in the white matter but is still detectable in normal gray matter. NeuN staining (blue) demonstrates neuronal cell bodies in the gray matter. Interestingly, cortical myeloarchitecture is identifiable on T_2*-weighted MRI. (*B*) EAE animal (M1) shows multiple cortical lesions on postmortem MRI corresponding to demyelinated areas on histology sections with sparing of neuronal somata. (*C*) EAE animal (M9) presents evident subpial and intracortical lesions on postmortem MRI corresponding to demyelinated areas on histology with preserved neuronal somata. Areas of normal-appearing gray matter (NAGM) are shown in the histology insets in the EAE animals (*B* and *C*).

lesions found on postmortem T_2*-weighted MRI images were also found on histology sections (Fig. 4), and lesion subtype classifications (leukocortical, intracortical, or subpial) were also the same. The three types of cortical lesions were characterized by a complete absence of PLP staining, interpreted as full demyelination, with persistence of the NeuN staining, interpreted as sparing of neuronal somata. In M10, a representative leukocortical lesion in the right parietal cortex is depicted in vivo, on postmortem MRI, and on histology (Fig. 5). This lesion presented a complete absence of PLP staining, with persistence of the NeuN staining (Fig. 5).

Discussion

Detecting cortical lesions routinely in MS patients with MRI remains a central challenge. The use of high-magnetic field strength MRI (≥3 T), optimized sequences, and high-spatial resolution, as well as a trained reader, are all necessary (Beck et al. 2018). However, even under optimal conditions, the natural history of cortical lesions is difficult to capture. Cortical lesions similar to those found in MS patients develop in marmoset EAE (Pomeroy et al. 2010; Kramann et al. 2015), but these have not previously been studied with MRI. As previously shown in MS patients (Mainero et al. 2009; Pitt et al. 2010; Cohen-Adad et al. 2011), T_2*-weighted images allowed us to detect different types of cortical lesions in marmoset EAE. Furthermore, we report that 70% of our animals with EAE presented at least one cortical lesion identified on postmortem T_2*-weighted MRI, and that an optimized high-resolution T_2*-weighted MRI sequence has reasonable (though imperfect) sensitivity for cortical lesion detection in vivo.

Similarly to cortical lesions in humans (Calabrese et al. 2010), the cortical lesions we detected in marmoset EAE were heterogeneous in type, size, and location. We commonly found these lesions in the cingulate, parietal, and frontal cortices, as well as in the parahippocampal gyrus. Interestingly, all identified leukocortical and intracortical lesions had a central vein detected as a dark line on T_2*-weighted images. Those veins ran centrally through the lesions and were also detected on histological sections, similar to what has been described for WM lesions in MS patients (Sati et al. 2016) and marmoset EAE (Gaitán et al. 2014).

Subpial lesions—the most elusive but potentially most significant type of cortical lesions—were more difficult to visualize than other cortical lesion subtypes on postmortem MRI. Indeed, these lesions showed faint hyperintense signal on T_2*-weighted images, with heterogeneous shapes and massive volume compared with the other cortical GM lesions. We could not identify central veins in subpial lesions, which traversed large areas of the cortex. Interestingly, the two animals with subpial lesions also had a longer course of EAE (16 and 18 weeks vs. a median of 11 weeks for all animals), although several other long-duration EAE marmosets showed no subpial lesions (e.g., M2). This result might suggest a different time course for subpial lesions compared with focal perivenular GM and WM lesions, but clearly, other factors must also play a role. Taken together, however, our results support the idea that diverse mechanisms drive the formation of different types of cortical lesions, originating from small parenchymal veins for focal leukocortical and intracortical lesions and leptomeninges for subpial lesions. This hypothesis is similar to what has been proposed in MS (Magliozzi et al. 2013; Junker et al. 2020).

Based on observations from the postmortem imaging and previous human studies (Geurts et al. 2005; Mainero et al. 2009; Cohen-Adad et al. 2011) at ultrahigh field, we focused on developing a T_2*-weighted sequence, with a reasonable AT for preclinical imaging (~1 h for six averages) and sufficiently high spatial resolution (125-µm isotropic) to be able to detect cortical lesions in vivo. A flow compensation approach was used in order to attenuate the signal coming from through-plane blood in vessels, allowing sufficiently high contrast-to-noise ratio for cortical lesions. Using this optimized protocol, we were able to detect in vivo leukocortical and intracortical lesions in two EAE marmosets (M10 and M11) and confirmed these results on postmortem MRI and histology in one animal (M10). In M10, no subpial lesions were detected either in vivo or postmortem. In M11, no subpial lesions were detected in vivo, but whether this is due to the relatively short duration of the EAE experiment (7 weeks) or a technical factor

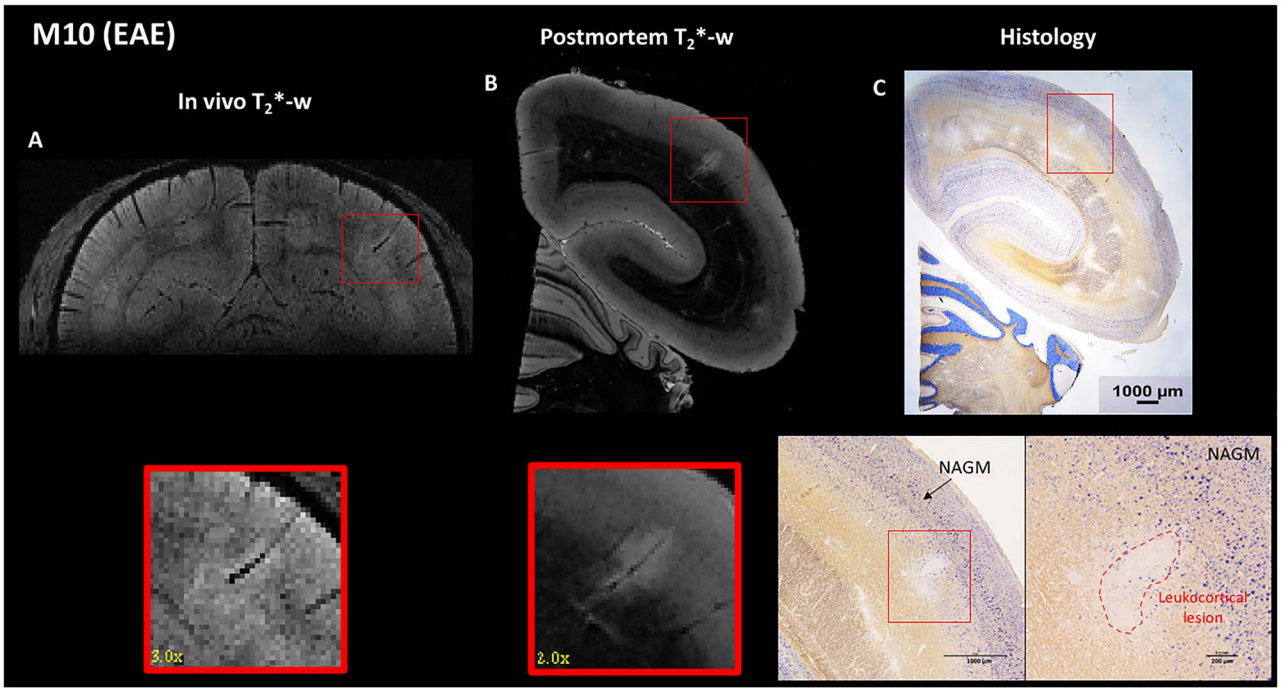

Figure 5. EAE animal (M10). A leukocortical lesion in the right parietal cortex (red box) was identified on (*A*) in vivo T_2*-weighted gradient echo MRI, (*B*) postmortem T_2*-weighted gradient echo MRI, and (*C*) histology sections with PLP/NeuN staining. Interestingly, cortical lesions appear larger in the in vivo images compared with postmortem images, likely due to water shifts. The lesion detected on MRI corresponds to a demyelinated area on histology (red dotted line, with absence of PLP staining), with sparing of neuronal somata (persistence of NeuN staining). An area of normal-appearing gray matter (NAGM) is identified in the histology inset (*C*).

hampering the in vivo detection of these lesions cannot be determined.

As observed in Figures 3 and 5, cortical lesions in M10 appeared larger on in vivo MRI versus postmortem MRI, likely due to the presence of edema that was only captured in vivo and was probably related to acute cortical lesion formation. Water present in vivo might have been washed out during the brain extraction and preparation for postmortem MRI.

Previous studies in MS patients showed the importance of cortical tissue damage, and mostly cortical demyelination, for the progression of physical and cognitive impairments (Calabrese et al. 2012; Harrison et al. 2015; Diker et al. 2016; Beck et al. 2018; Forslin et al. 2018; Magliozzi et al. 2018). Extensive statistical analysis was not undertaken in this study due to the small number of animals used, but the severity of EAE score at the terminal scan and the number/total volume of GM lesions seems to be linked (correlation coefficients of 0.92 and 0.7, respectively) (Fig. 2). No significant correlations between cortical lesion volume/number and disease duration were found.

In this study, access to brain tissues enabled us to validate our MRI findings and avoid any potential misinterpretation caused by MRI-related artifacts. We found good agreement between the hyperintense cortical lesions identified on both in vivo and postmortem MRI and cortical demyelinated lesions identified on histology sections. Interestingly, the neuronal somata appear to be preserved in cortical lesions. Even though T_2* contrast can be sensitive to different pathophysiological mechanisms, our observations corroborate its reasonably high sensitivity to demyelination, a point already demonstrated by previous studies investigating the correlation between MRI and myelin in spinal cord postmortem tissues (Schmierer et al. 2018; Lefeuvre et al. 2019).

This study has some limitations. Among them, there was significant variability in cortical lesion formation across the 10 animals (seven with cortical lesions) studied, some heterogeneity of immunization type and hemispheres available (a common situation in marmoset EAE studies, where scarce animals are often used for multiple studies simultaneously), lack of serial in vivo images to follow the spatiotemporal evolution of WM and GM lesions, and limited histological analysis.

By using ultrahigh-resolution T_2*-weighted MRI in vivo and postmortem, we were able to visualize cortical lesions in a marmoset model of MS. As in MS, three types of cortical lesions were observed by MRI in marmoset EAE, as previously described only histopathologically. Our imaging findings were confirmed by histology, revealing substantial cortical demyelination in the cortex of some of the diseased animals, with sparing of neuronal somata within most lesions. Our study emphasizes the relevance of our marmoset model to study mechanisms and dynamics of cortical pathology in MS.

Supplementary Material

Supplementary material can be found at *Cerebral Cortex* online.

Funding

This research was supported by the Intramural Research Program of National Institute of Neurological Disorders and Stroke/National Institutes of Health [Z01NS0003119], by the Adelson Medical Research Foundation, and by two fellowship grants from the National Multiple Sclerosis Society (Clinician Scientist Development Award [FAN-1507-05500] and Career Transition Fellowship [TA-1805-31038]).

Notes

The authors thank Sam Antonio and Dr James O'Malley in the NINDS animal facility for marmoset care and support in animal management; Daniel Abraham and Dr Seung Kwon Ha for help in the histology portion of the study; Dr Omar Al-Louzi for support in the data processing portion; and Roger Depaz for help in the data acquisition and animal care. The study was presented in part at the 27th annual meeting of the International Society for Magnetic Resonance in Medicine (Montreal, 2019). *Conflict of Interest*: Dr. Daniel S. Reich has received research funding from Vertex Pharmaceuticals.

References

Absinta M, Sati P, Reich DS. 2016. Advanced MRI and staging of multiple sclerosis lesions. *Nat Rev Neurol*. 12:358–368.

Ascherio A, Munger KL. 2016. Epidemiology of multiple sclerosis: from risk factors to prevention-an update. *Semin Neurol*. 36:103–114.

Beck ES, Sati P, Sethi V, Kober T, Dewey B, Bhargava P, Nair G, Cortese IC, Reich DS. 2018. Improved visualization of cortical lesions in multiple sclerosis using 7T MP2RAGE. *Am J Neuroradiol*. 39:459–466.

Bø L, Vedeler CA, Nyland HI, Trapp BD, Mørk SJ. 2003. Subpial demyelination in the cerebral cortex of multiple sclerosis patients. *J Neuropathol Exp Neurol*. 62:723–732.

Burrows DJ, McGown A, Jain SA, De Felice M, Ramesh TM, Sharrack B, Majid A. 2019. Animal models of multiple sclerosis: from rodents to zebrafish. *Mult Scler*. 25:306–324.

Calabrese M, Filippi M, Gallo P. 2010. Cortical lesions in multiple sclerosis. *Nat Rev Neurol*. 6:438–444.

Calabrese M, Poretto V, Favaretto A, Alessio S, Bernardi V, Romualdi C, Rinaldi F, Perini P, Gallo P. 2012. Cortical lesion load associates with progression of disability in multiple sclerosis. *Brain*. 135:2952–2961.

Cohen-Adad J, Benner T, Greve D, Kinkel RP, Radding A, Fischl B, Rosen BR, Mainero C. 2011. In vivo evidence of disseminated subpial T2* signal changes in multiple sclerosis at 7 T: a surface-based analysis. *Neuroimage*. 57:55–62.

Diker S, Has AC, Kurne A, Göçmen R, Oğuz KK, Karabudak R. 2016. The association of cognitive impairment with gray matter atrophy and cortical lesion load in clinically isolated syndrome. *Mult Scler Relat Disord*. 10:14–21.

Dutta R, Trapp BD. 2007. Pathogenesis of axonal and neuronal damage in multiple sclerosis. *Neurology*. 68:S22–S31.

Forslin Y, Bergendal Å, Hashim F, Martola J, Shams S, Wiberg MK, Fredrikson S, Granberg T. 2018. Detection of leukocortical lesions in multiple sclerosis and their association with physical and cognitive impairment: a comparison of conventional and synthetic phase-sensitive inversion recovery MRI. *Am J Neuroradiol*. 39:1995–2000.

Gaitán MI, Maggi P, Wohler J, Leibovitch E, Sati P, Calandri IL, Merkle H, Massacesi L, Silva AC, Jacobson S *et al*. 2014. Perivenular brain lesions in a primate multiple sclerosis model at 7-tesla magnetic resonance imaging. *Mult Scler*. 20:64–71.

Geurts JJG, Bö L, Pouwels PJW, Castelijns JA, Polman CH, Barkhof F. 2005. Cortical lesions in multiple sclerosis: combined postmortem MR imaging and histopathology. *Am J Neuroradiol*. 26:572–577.

Guy J, Sati P, Leibovitch E, Jacobson S, Silva A, Reich D. 2016. Custom fit 3D-printed brain holders for comparison of histology with MRI in marmosets. *J Neurosci Methods*. 257:55–63.

Harrison DM, Roy S, Oh J, Izbudak I, Pham D, Courtney S, Caffo B, Jones CK, van Zijl P, Calabresi PA. 2015. Association of cortical lesion burden on 7-T magnetic resonance imaging with cognition and disability in multiple sclerosis. *JAMA Neurol*. 72:1004–1012.

Junker A, Wozniak J, Voigt D, Scheidt U, Antel J, Wegner C, Brück W, Stadelmann C. 2020. Extensive subpial cortical demyelination is specific to multiple sclerosis. *Brain Pathol*. 30:641–652.

Kramann N, Neid K, Menken L, Schlumbohm C, Stadelmann C, Fuchs E, Brück W, Wegner C. 2015. Increased meningeal T and plasma cell infiltration is associated with early subpial cortical demyelination in common marmosets with experimental autoimmune encephalomyelitis. *Brain Pathol*. 25: 276–286.

Kutzelnigg A, Lassmann H. 2005. Cortical lesions and brain atrophy in MS. *J Neurol Sci*. 233:55–59.

Lee NJ, Ha S-K, Sati P, Absinta M, Luciano NJ, Lefeuvre JA, Schindler MK, Leibovitch EC, Ryu JK, Petersen MA *et al*. 2018. Spatiotemporal distribution of fibrinogen in marmoset and human inflammatory demyelination. *Brain*. 141: 1637–1649.

Lefeuvre JA, Guy JR, Luciano NJ, Ha S-K, Leibovitch E, Santin MD, Silva AC, Jacobson S, Lehéricy S, Reich DS *et al*. 2019. The spectrum of spinal cord lesions in a primate model of multiple sclerosis. *Mult Scler*. 26:284–293.

Lucchinetti CF, Popescu BFG, Bunyan RF, Moll NM, Roemer SF, Lassmann H, Brück W, Parisi JE, Scheithauer BW, Giannini C, et al. 2011. Inflammatory cortical demyelination in early multiple sclerosis. *N Engl J Med* 365:2188–2197.

Luciano NJ, Sati P, Nair G, Guy JR, Ha S-K, Absinta M, Chiang W-Y, Leibovitch EC, Jacobson S, Silva AC *et al*. 2016. Utilizing 3D printing technology to merge MRI with histology: a protocol for brain sectioning. *J Vis Exp*. 118:54780.

Maggi P, Macri SMC, Gaitán MI, Leibovitch E, Wholer JE, Knight HL, Ellis M, Wu T, Silva AC, Massacesi L *et al*. 2014. The formation of inflammatory demyelinated lesions in cerebral white matter. *Ann Neurol*. 76:594–608.

Maggi P, Sati P, Massacesi L. 2017. Magnetic resonance imaging of experimental autoimmune encephalomyelitis in the common marmoset. *J Neuroimmunol*. 304:86–92.

Magliozzi R, Reynolds R, Calabrese M. 2018. MRI of cortical lesions and its use in studying their role in MS pathogenesis and disease course. *Brain Pathol*. 28:735–742.

Magliozzi R, Serafini B, Rosicarelli B, Chiappetta G, Veroni C, Reynolds R, Aloisi F. 2013. B-cell enrichment and Epstein-Barr virus infection in inflammatory cortical lesions in secondary progressive multiple sclerosis. *J Neuropathol Exp Neurol*. 72:29–41.

Mainero C, Benner T, Radding A, van der Kouwe A, Jensen R, Rosen BR, Kinkel RP. 2009. In vivo imaging of cortical pathology in multiple sclerosis using ultra-high field MRI. *Neurology*. 73:941–948.

Papoti D, Yen CC-C, Hung C-C, Ciuchta J, Leopold DA, Silva AC. 2017. Design and implementation of embedded 8-channel receive-only arrays for whole-brain MRI and fMRI of conscious awake marmosets: 8-channel receive-only embedded arrays for MRI/fMRI of awake marmosets. *Magn Reson Med*. 78:387–398.

Pitt D, Boster A, Pei W, Wohleb E, Jasne A, Zachariah CR, Rammohan K, Knopp MV, Schmalbrock P. 2010. Imaging cortical lesions in multiple sclerosis with ultra-high-field magnetic resonance imaging. *Arch Neurol*. 67:812–818.

Pomeroy IM, Jordan EK, Frank JA, Matthews PM, Esiri MM. 2008. Diffuse cortical atrophy in a marmoset model of multiple sclerosis. *Neurosci Lett*. 437:121–124.

Pomeroy IM, Jordan EK, Frank JA, Matthews PM, Esiri MM. 2010. Focal and diffuse cortical degenerative changes in a marmoset model of multiple sclerosis. *Mult Scler*. 16:537–548.

Reich DS, Lucchinetti CF, Calabresi PA. 2018. Multiple sclerosis. *N Engl J Med*. 378:169–180.

Sati P, Oh J, Constable RT, Evangelou N, Guttmann CRG, Henry RG, Klawiter EC, Mainero C, Massacesi L, McFarland H *et al*. 2016. The central vein sign and its clinical evaluation for the diagnosis of multiple sclerosis: a consensus statement from the North American Imaging in Multiple Sclerosis Cooperative. *Nat Rev Neurol*. 12:714–722.

Schmierer K, McDowell A, Petrova N, Carassiti D, Thomas DL, Miquel ME. 2018. Quantifying multiple sclerosis pathology in postmortem spinal cord using MRI. *Neuroimage*. 182:251–258.

Stüber C, Pitt D, Wang Y. 2016. Iron in multiple sclerosis and its noninvasive imaging with quantitative susceptibility mapping. *Int J Mol Sci*. 17:100.

't Hart BA, Massacesi L. 2009. Clinical, pathological, and immunologic aspects of the multiple sclerosis model in common marmosets (*Callithrix jacchus*). *J Neuropathol Exp Neurol*. 68: 341–355.

Tang MY, Chen TW, Zhang XM, Huang XH. 2014. GRE T2$*$-weighted MRI: principles and clinical applications. *Biomed Res Int*. 2014:312142.

Villoslada P, Hauser SL, Bartke I, Unger J, Heald N, Rosenberg D, Cheung SW, Mobley WC, Fisher S, Genain CP. 2000. Human nerve growth factor protects common marmosets against autoimmune encephalomyelitis by switching the balance of T helper cell type 1 and 2 cytokines within the central nervous system. *J Exp Med*. 191: 1799–1806.